

## SPECTROSCOPIC AND STRUCTURAL PROPERTIES OF TeO<sub>2</sub>-ZnO-Na<sub>2</sub>O-Er<sub>2</sub>O<sub>3</sub>-Au GLASSES

S. K. GHOSHAL, ASMAHANI AWANG\*, M. R. SAHAR, RAJA J. AMJAD,  
M. REZA DOUSTI

*Advanced Optical Materials Research Group, Department of Physics, Faculty of Science, Universiti Teknologi Malaysia, 81310 UTM Skudai, Johor, Malaysia*

This paper reports the spectroscopic and structural properties of glasses with composition 70TeO<sub>2</sub>-20ZnO-10Na<sub>2</sub>O-(x)Er<sub>2</sub>O<sub>3</sub>-0.2Au (x=0.5, 1.0 and 1.5) synthesized using melt-quenching technique. The physical and thermal properties of glass samples with different Er<sub>2</sub>O<sub>3</sub> contents are found to vary due to structural changes. The absorption spectra consist of seven bands attributed to the absorption from ground state (<sup>4</sup>I<sub>15/2</sub>) to various excited states of 4f shell. TEM micrograph confirms the presence of gold nanoparticles (Au NPs) with average size ~ 7.6 nm. The observed visible up-conversion (UC) emission under 779 nm excitation wavelength exhibits three bands centered at 533 nm (green), 547 nm (green) and 637 nm (red). The glass with 1.0 mol% Er<sub>2</sub>O<sub>3</sub> displays dominant enhancement (two fold) in the UC emission intensity for the green band (<sup>4</sup>S<sub>3/2</sub>→<sup>4</sup>I<sub>15/2</sub>) and relatively weaker enhancement for the red band (<sup>4</sup>F<sub>9/2</sub>→<sup>4</sup>I<sub>15/2</sub>). The enhancement is primarily ascribed to the energy transfer between Er<sup>3+</sup> ions and local field effect of Au NPs. The IR result reveals shifts of the peaks due to the incorporation of Er<sub>2</sub>O<sub>3</sub> of varying concentration that consequently change the bonding between ligands in the glass matrix. Our results suggest that the proposed glasses can be nominated as potential materials for the developments of optical devices.

(Received June 18, 2013; Accepted October 29, 2013)

*Keywords:* Gold nanoparticles, TEM, Up-conversion, Surface plasmon resonance, Tellurite glass

### 1. Introduction

The tellurium oxide (TeO<sub>2</sub>) based glasses are attractive because they can be doped with large concentration of rare-earth (RE) ions compared to other oxide glasses [1, 2]. The tellurite glasses containing high concentrations of RE ions are promising for the applications in optical data transmission, detection, sensing and lasing [3]. Tellurite glasses are highly potential as the host material in comparison to silicate, borate and phosphate glasses due to their large transmission window (360-6500 nm), relative low-phonon energy (~700 cm<sup>-1</sup>), large nonlinear optical response, high refractive index values (~2), high dielectric constant, good corrosion resistance, high thermal and chemical stability to cite a few [4, 5].

The trivalent Er<sup>3+</sup> ion is one of the most widely exploited RE ions because its favorable energy level structure offers simultaneous green and red emissions for laser actions. However, the small absorption cross section of the RE ions such as Er<sup>3+</sup> disqualifies them to be a strong emitters [6]. In the case of RE luminescent centers, the coupling between centers and the lattice is relatively weak because the 4f electrons are shielded by 5s and 5p electrons [2]. The weak absorption cross section of the RE ions affects the UC efficiency where more than one photon is required to generate a higher energy up-converted emission [7, 8]. Several methods are proposed to improve the luminescence of RE [9]. Firstly, the addition of the second dopant (either alternative REs or

---

\* Corresponding author: asmahani\_awang@yahoo.com

transition metals) aimed to improve the optical properties of RE-doped glasses [7, 8]. The alternative method to overcome the restriction is introduced by coupling RE ions with plasmonic nanoclusters to enhance the luminescence intensity of RE ions [6, 10]. The potential of plasmonic metal NPs can confine the electromagnetic energy or optical excitation in a nanoscale volume (called localized surface plasmon) and thereby mediate strong optical interactions within this volume by local electric field enhancements [6, 10, 11].

Nanometals are plasmas, comprising of fixed positive ion cores and oscillating conduction electrons whose resonant frequency arises from the restoring force exerted by the altered charge distribution on the mobile charges during their displacement from equilibrium [12]. Recently, interactions between RE ions and metallic NPs in glass generated renewed interest due to their unique ability to enhance the spectroscopic properties for efficient optical devices [5, 10, 13]. Despite much effort, the mechanism behind the interaction of metallic NPs with RE ions in the glass matrix in improving the structural and optical properties are still lacking. We incorporate Au NPs into the tellurite glass matrix to examine the interaction between metal nanoclusters with  $\text{Er}^{3+}$  ions. The spectroscopic and structural properties of glasses in the presence of Au NPs are studied by manipulating varying concentration of  $\text{Er}_2\text{O}_3$  that unfolds the interactions between excess RE ions and the ligands.

## 2. Experimental

The  $\text{Er}^{3+}$  doped nanogold tellurite glasses were synthesized by the conventional melt quenching method. The starting materials with high purity of  $\text{TeO}_2$ ,  $\text{ZnO}$ ,  $\text{Na}_2\text{O}$ ,  $\text{Er}_2\text{O}_3$  and Au were mixed thoroughly. The compositions were taken within the glass forming region and are summarized in Table 1. A platinum crucible containing the glass constituents was placed in a furnace from room temperature up to  $900\text{ }^\circ\text{C}$  for 25 min. The melt was then casted in a brass mold after melting process. Subsequently, the sample was transferred to an annealing furnace and kept for 3 h at  $295\text{ }^\circ\text{C}$  to remove completely the thermal and mechanical strains. The samples were then allowed to cool to room temperature. Finally, the samples were cut and polished for the structural and optical measurements. Density of prepared glasses was determined by Archimedes method (Analytical balance with specific density-Precisa XT 220 A) using toluene ( $\rho = 0.8669\text{ g cm}^{-3}$ ) as an immersion liquid. The X-ray diffraction (XRD) was performed using Rigaku-Rota Flex mod RU200B (at a wavelength  $1.5406\text{ \AA}$  Cu  $K\alpha$ ). Absorption spectra were recorded by employing Shimadzu UV-3101PC scanning spectrophotometer (Kyoto, Japan), in range of 400 - 1800 nm. Energy dispersive X-ray spectroscopy (EDX) system model Oxford INCA Energy 200 was used to display the elemental occurrence in our glass materials. Transmission Electron Microscopic (TEM) analyses was performed using a Philips CM12 operating at 200 kV. The emission spectra were recorded by Perkin Elmer LS-55 photoluminescence (PL) spectrometer (UK). The Fourier Transform Infrared (FTIR) spectra of fine powder of glasses mixed with KBR were obtained by using a Perkin Elmer Spectrum One FT-IR spectrometer. All measurements were carried out at room temperature.

Table 1. Nomenclatures and nominal compositions for respective glass samples.

Sample	Nominal compositions
TZNE0.5-Au	70 $\text{TeO}_2$ -20 $\text{ZnO}$ -10 $\text{Na}_2\text{O}$ -0.5 $\text{Er}_2\text{O}_3$ -0.2Au
TZNE1.0-Au	70 $\text{TeO}_2$ -20 $\text{ZnO}$ -10 $\text{Na}_2\text{O}$ -1.0 $\text{Er}_2\text{O}_3$ -0.2Au
TZNE1.5-Au	70 $\text{TeO}_2$ -20 $\text{ZnO}$ -10 $\text{Na}_2\text{O}$ -1.5 $\text{Er}_2\text{O}_3$ -0.2Au

### 3. Results and discussion

Fig. 1(a) displays the XRD pattern of the glass samples TZNE0.5-Au which indicates the amorphous nature in the presence of a broad hump located between 25° and 35° degrees [10]. Fig.1 (b) shows the corresponding EDX spectra in the presence of Au NPs in the glass matrix. Various physical and inter-nuclear properties of our glass samples are enlisted in Table 2. In this present study, the Au is presumably dissolved as  $\text{Au}^+$  in glass matrix [14]. The annealing at 300 °C (based on  $T_g$ ) led to the diffusion of  $\text{Au}^+$  ions in the vitreous matrix that causes the reduction of these ions to  $\text{Au}^0$  to form and grow Au NPs [13, 15]. These mechanisms are supported by the work of Qiu [16], where the role of neutralized metallic NPs to promote nucleation is emphasized. Refer to Table 2, further addition of  $\text{Er}_2\text{O}_3$  content decreases the refractive index and increases the density of glasses. The participation of  $\text{Er}^{3+}$  ions in the glass matrix induce structural changes [17] and led to the formation of greater number of non-bridging oxygen (NBO) [11]. In addition, the presence of Au NPs in the glass matrix reduces the number of NBO which in turn decrease the refractive index [18]. This behavior is related to the mechanism in which the  $\text{Au}^+$  captures the electron to form an Au atom [16]. The decrement in the population of NBO, consequently strengthen the glass structure responsible for the increment of the density [19].

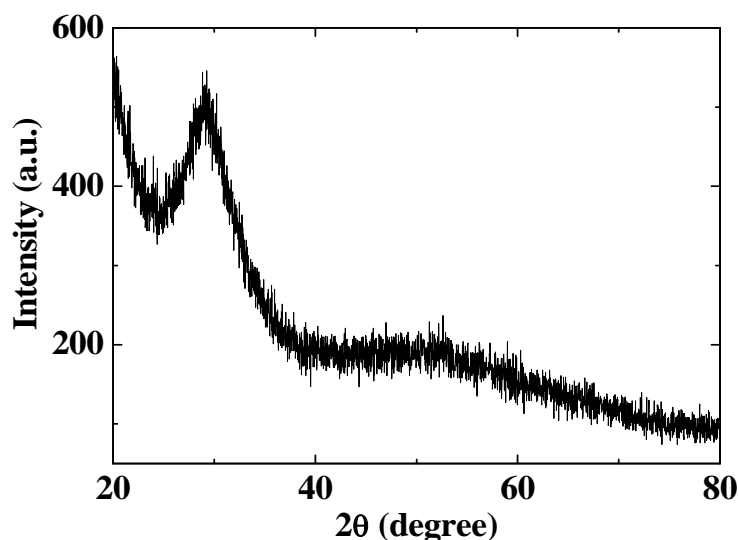


Fig.1 (a). XRD spectra of TZNE0.5-Au sample.

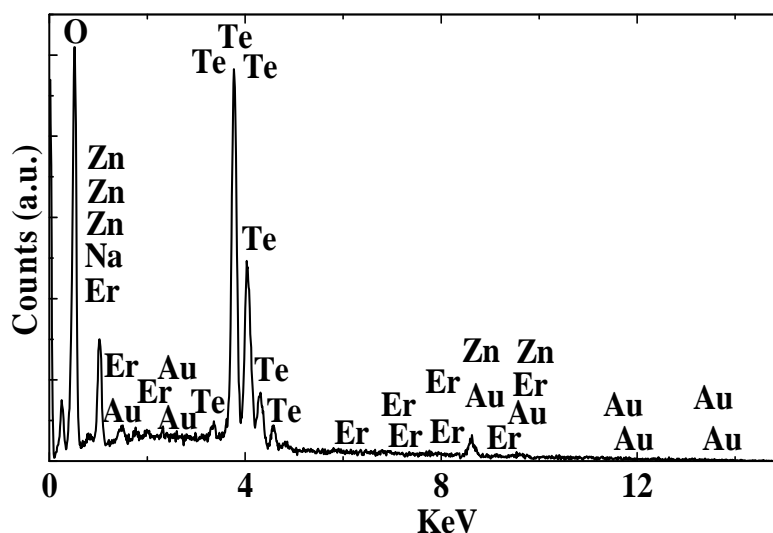


Fig.1 (b). EDX spectra of TZNE0.5-Au.

Table 2. Glass labels, designation of their refractive index ( $n$ ), density ( $\rho$ ,  $\text{g.cm}^{-3}$ ) and inter-nuclear properties.

Topic	Corresponding values		
Glass label	TZNE0.5-Au	TZNE1.0-Au	TZNE1.5-Au
Density ( $\text{g.cm}^{-3}$ )	5.189	5.190	5.193
Refractive index	2.379	2.374	2.373
Concentration of Au (wt%)	0.2	0.2	0.2
Au NPs concentration, $N \times 10^{19}$ (atoms/ $\text{cm}^3$ )	4.58	4.51	4.46
Concentration of $\text{Er}_2\text{O}_3$ (wt%)	0.5	1.0	1.5
$\text{Er}^{3+}$ ion concentration, $N \times 10^{19}$ (ions/ $\text{cm}^3$ )	11.44	22.57	33.42
Au-Au distance, $d$ (Å)	27.95	28.09	28.20
$\text{Er}^{3+}$ - $\text{Er}^{3+}$ distance (Å)	20.60	16.42	14.41
Au- $\text{Er}^{3+}$ distance (Å)	31.27	29.85	29.40
Relative separation, $d/D$	0.36	0.37	0.38

The electronic absorptions in erbium ions are attributed to 4f-4f transitions. The absorption spectra of  $\text{Er}^{3+}$  ions corresponding to transitions starting from the ground state ( $^4I_{15/2}$ ) to the excited states [5, 11] are illustrated in Fig. 2(a). The bands centered at 448, 488, 523, 655, 800, 997 and 1533 nm are attributed to the  $^4I_{15/2} \rightarrow ^4F_{5/2}$ ,  $^4I_{15/2} \rightarrow ^4F_{7/2}$ ,  $^4I_{15/2} \rightarrow ^2H_{11/2}$ ,  $^4I_{15/2} \rightarrow ^4F_{9/2}$ ,  $^4I_{15/2} \rightarrow ^4I_{9/2}$ ,  $^4I_{15/2} \rightarrow ^4I_{11/2}$ , and  $^4I_{15/2} \rightarrow ^4I_{13/2}$  electronic transitions, respectively. A weak peak at around 540 nm can be ascribed to the transition from ground state to  $^4S_{3/2}$  excited state. Fig. 2(b) shows DTA thermogram of all glass samples in the range of 0-800 °C. Refer to Table 2, the glass transition temperature ( $T_g$ ), the onset temperature of crystallization ( $T_x$ ), and the crystallization temperature ( $T_c$ ) are all shifted with the increase of  $\text{Er}_2\text{O}_3$  contents. Higher concentration of  $\text{Er}^{3+}$  ions decreases the glass transition temperature [20] from 320 to 221°C. Moneim et al. [21] proposed that this behavior results as a decrease in the rigidity of the network. The variations in  $T_g$  is possibly due to the change in RE ions ( $\text{Er}_2\text{O}_3$  our case) concentrations that get re-arranged in the glass as reported [21]. The increasing value of  $T_c - T_g$  implies that the structural glass units become stronger when the oxide components are added [22]. The stability of tellurite glasses can be determined by using Hruby parameter [11];

$$H = \frac{(T_x - T_g)}{T_g}$$

The increasing value of  $H$  from 0.67 to 0.85 with the addition of higher  $\text{Er}_2\text{O}_3$  content represents the better glass forming ability.

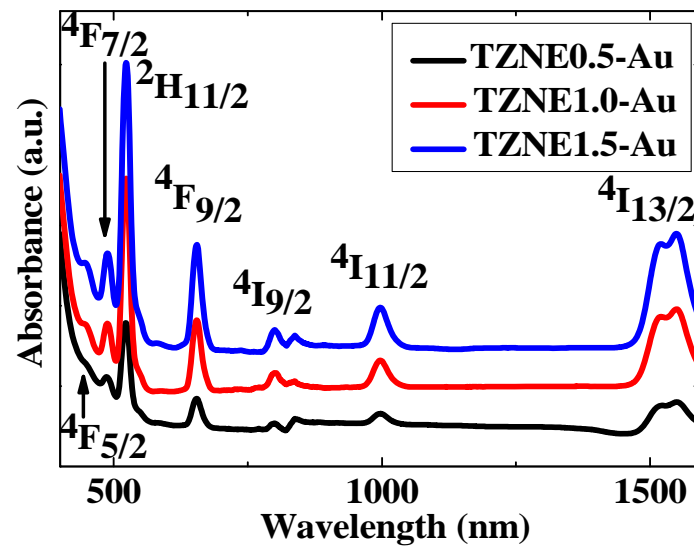


Fig.2 (a). Absorption spectra.

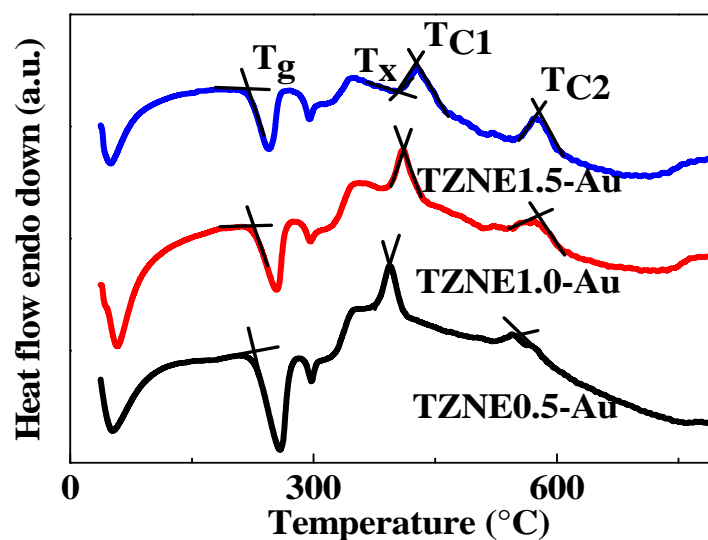


Fig.2 (b). DTA thermograph of all glass samples.

The representative TEM image of TZNE0.5-Au glass sample (Fig. 3(a)) clearly shows quasi-spherical shaped randomly oriented Au NPs. The major axis (longitudinal) of the marked NPs ranges from 3 to 11 nm while minor axis varies between 2 and 8 nm. Their mean aspect ratio is in the range of 1.2-1.5. The existence of quasi-particles is also reported by Som et al. [10] in their study on enhanced fluorescence in antimony glass hybrid. The average size of the gold NPs is estimated to be  $\sim 7.6$  nm with a Gaussian distribution, as illustrated in Fig. 3 (b).

The room temperature PL spectra under excitation of 779 nm wavelength for all samples as presented in Figure 4(a). Three emission bands evidenced at 533, 547 and 637 nm are ascribed to  ${}^2H_{11/2} \rightarrow {}^4I_{15/2}$ ,  ${}^4S_{3/2} \rightarrow {}^4I_{15/2}$  and  ${}^4F_{9/2} \rightarrow {}^4I_{15/2}$  transitions, respectively. A relatively weaker band is appeared at 637 nm (red). The most prominent up-converted green peak is located at 547 nm (green). The glass with 1.0 mol%  $Er_2O_3$  shows the largest intensity in the entire spectral range with two folds enhancement. Interestingly, further addition of  $Er_2O_3$  (glass TZEA1.5-Au) results a quenching in the intensity of UC emissions. Similar behavior is reported by Kumar et al. [23] in their study of luminescence properties in ternary glasses, where the quenching is observed beyond

1.0 mol% of the  $\text{Er}_2\text{O}_3$  concentration. It is worth mentioning that the increase in intensity of the red emission centered at 637 nm ( ${}^4\text{F}_{9/2} \rightarrow {}^4\text{I}_{15/2}$ ) relative to the green emission with the increase of  $\text{Er}^{3+}$  ions concentration is attributed to the energy transfer (ET) between excited ions [2].

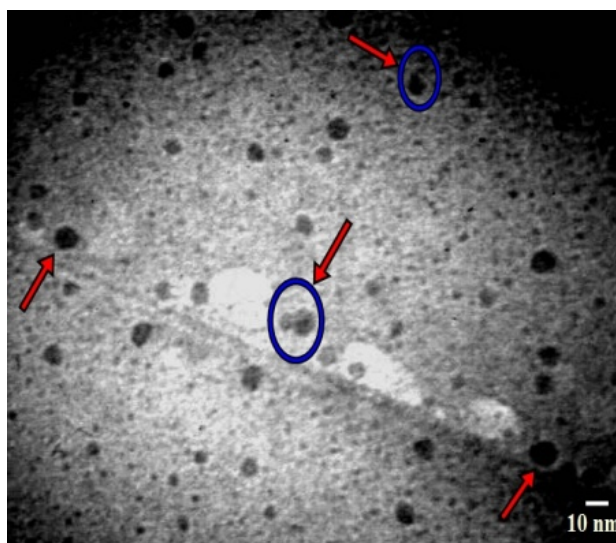


Fig.3 (a). TEM image showed the distribution of Au NPs dispersed in the glass matrix.

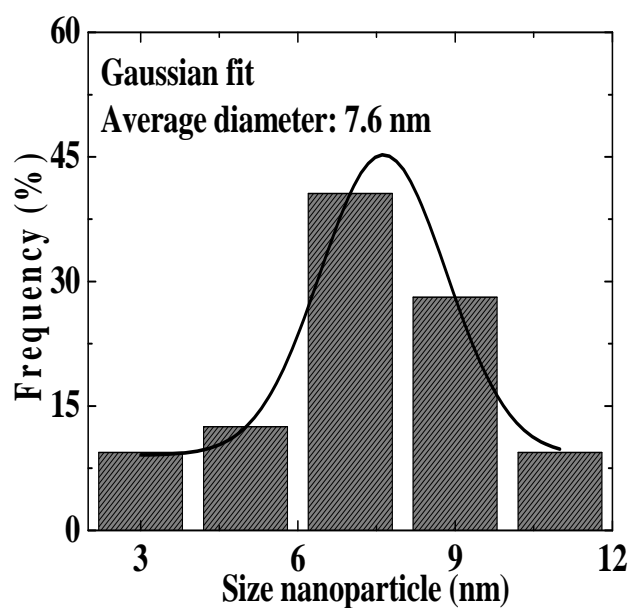
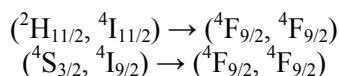


Fig.3 (b). Histogram for the abundance of nanoparticles for TZNE0.5-Au sample.

Fig. 4(b) illustrates the schematic representation of energy level diagram of  $\text{Er}^{3+}$  ions. In the first mechanism, a resonating photon at 779 nm excitation stimulates the erbium ion and the  ${}^4\text{I}_{9/2}$  level is populated through the ground state absorption (GSA) wherein nonradiative relaxation (NR) to  ${}^4\text{I}_{11/2}$  level occurs. Absorption of another 779 nm laser photon by the  ${}^4\text{I}_{11/2}$  excited state excites the ion to  ${}^4\text{F}_{3/2}$  state via excited state absorption (ESA). Subsequently, the nonradiative multi-phonon relaxations from the metastable  ${}^4\text{F}_{3/2}$  state populate the lower-lying levels of  ${}^2\text{H}_{11/2}$ ,  ${}^4\text{S}_{3/2}$  and  ${}^4\text{F}_{9/2}$  [2, 24]. In the intermediate energy level the ET occurs between two  $\text{Er}^{3+}$  ions. The

cooperative ET (CET) process can operate between two nearby  $\text{Er}^{3+}$  ions at higher concentration of  $\text{Er}^{3+}$  [23];



An ion in  $^4\text{S}_{3/2}$  level decays to  $^4\text{F}_{9/2}$  level and its excess energy is taken up by an ion in the  $^4\text{I}_{9/2}$  state to excite the later to the  $^4\text{F}_{9/2}$  state [18]. Energy transfer between two neighboring  $\text{Er}^{3+}$  ions is also probable through two different mechanism: (1) a nonradiative decay from  $^4\text{I}_{11/2}$  to ground state excites the neighboring ion from  $^4\text{I}_{13/2}$  to  $^2\text{H}_{11/2}$  levels; (2) another ET process may occur where two electrons in the  $^4\text{I}_{11/2}$  excited state of different ions contribute to one nonradiative emission from  $^4\text{I}_{11/2}$  to ground state that in turn transfer the energy to another one to excite to  $^2\text{H}_{11/2}$  excited state [25].

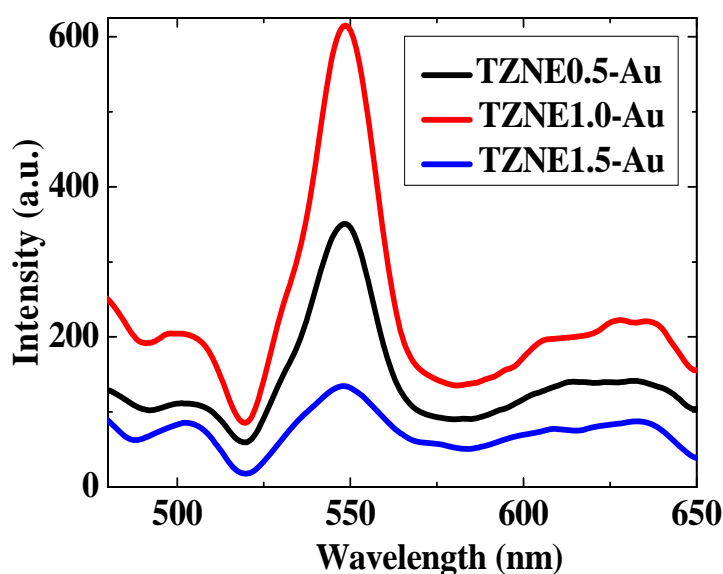


Fig.4 (a). Up-conversion emission spectra of glass samples under  $\lambda_{\text{exc}}=779$  nm.

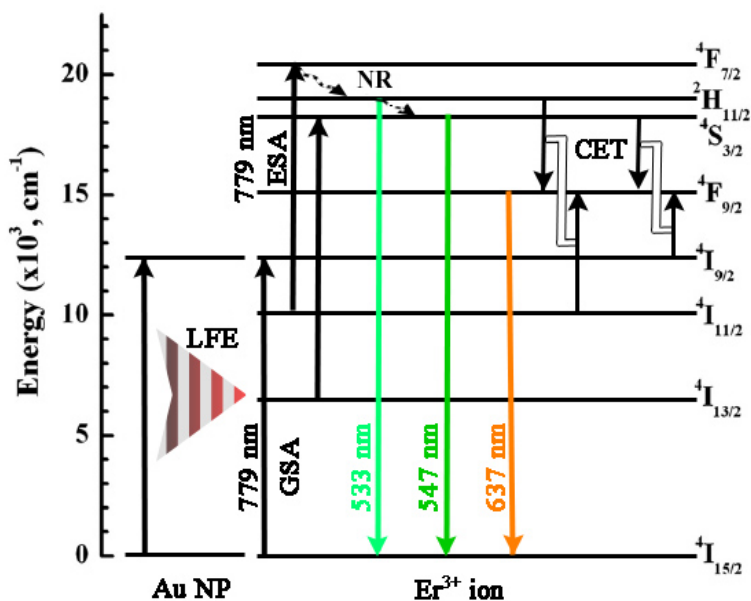


Fig.4 (b). Schematic energy level diagram of  $\text{Er}^{3+}$  ion in  $\text{TeO}_2\text{-ZnO-Na}_2\text{O-Er}_2\text{O}_3\text{-Au}$  glass.

At lower concentration, the  $\text{Er}^{3+}$  ions are usually randomly distributed in the host lattice, which led to the occurrence of  $^4\text{S}_{3/2}$  or  $^2\text{H}_{11/2}$  levels to decay mostly radiatively to  $^4\text{I}_{15/2}$ . The higher intensity associated with the green emission as observed in the PL results for TZNE1.0-Au glass sample is in fact related to this radiative decay. There is also a possibility of the enhancement in the PL intensity due to the increased local field results from the mismatch of the dielectric function of the metallic NPs (Au NPs in present study) and the glasses as reported by Kassab et al. [26]. The local field effect of Au NPs emerges from localized surface plasmon resonance is also responsible for such enhancement. However, at higher concentration, some of the  $\text{Er}^{3+}$  ions are surrounded by more nearest neighbor than others which is responsible for the concentration quenching (Refer to Table 2, the  $\text{Er}^{3+}$ - $\text{Er}^{3+}$  distance become closer with increasing  $\text{Er}_2\text{O}_3$  content). Under this condition, the luminescence lifetime of  $^4\text{S}_{3/2}$  and  $^2\text{H}_{11/2}$  levels is shortened as a result of the cross-relaxation processes. The cross-relaxation process is dominant at higher concentration of  $\text{Er}^{3+}$  ions and subsequently led to the quenching of the emission intensity [27].

Fig. 5 shows the recorded absorption bands in the IR region of all glass samples. The assignments of all the transmission peaks for the studied glass samples are summarized in Table 3. The origin of broad bands are due to the combined effects of higher degeneracy of vibrational states, thermal broadening of the lattice dispersion and mechanical scattering of the powdered samples [28]. The characteristics bands of  $\text{TeO}_4$  are in spectral range of  $350\text{-}800\text{ cm}^{-1}$  as reported earlier [23]. The occurrence of the peak around  $466\text{-}471\text{ cm}^{-1}$  (indicated in Table 4) is attributed to the Zn-O tetrahedral bond and the appearance of several weak peaks occur within these ranges might be due to the deformation of the Te-O bond vibration [29].

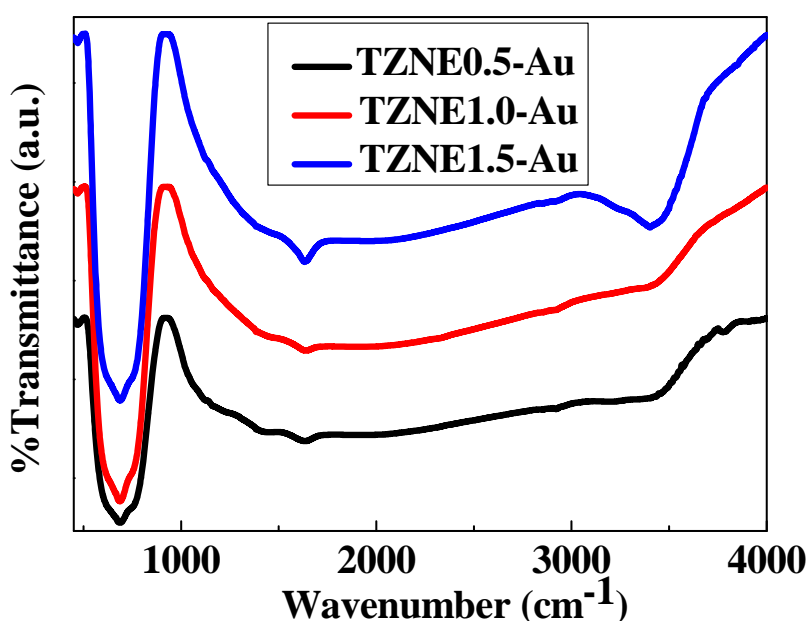


Fig.5. The IR spectra of  $\text{TeO}_2\text{-Er}_2\text{O}_3\text{-ZnO-Na}_2\text{O-Au}$  glass samples.

Table 3. Thermal parameters of  $\text{Er}^{3+}$  doped nanogold tellurite glasses.

Glass	$T_g$ (°C)	$T_x$ (°C)	$T_{C1}$ (°C)	$T_{C2}$ (°C)	$T_C - T_g$ (°C)	H
TZNE0.5-Au	225	376	394	550	169	0.67
TZNE1.0-Au	224	390	410	575	186	0.74
TZNE1.5-Au	219	405	428	577	209	0.85

Table 4. IR band assignments for the  $\text{TeO}_2$ - $\text{Er}_2\text{O}_3$ - $\text{ZnO}$ - $\text{Na}_2\text{O}$ - $\text{Au}$  glass samples.

Glass samples			Band assignments
TZN0.5-Au	TZNE1.0-Au	TZNE1.5-Au	
466	471	471	Vibrations of Zn-O tetrahedral bond ( $\text{ZnO}_4$ )
667	664	664	Symmetric stretching vibrations of Te-O in $\text{TeO}_4$
687	688	690	Te-O bending vibrations in $\text{TeO}_3$ units
1128	-	-	Te-O-Zn linkages
1635	1637	1640	Vibrations of water molecule
2921	2925	2928	Hydrogen bonding
3428	3429	3432	Fundamental stretching of hydroxyl group

Pavani et al. [30] reported that the absorption band of  $\text{TeO}_3$  and  $\text{TeO}_4$  group, in general, is correlated to the frequency range of  $650\text{-}700\text{ cm}^{-1}$  and  $600\text{-}650\text{ cm}^{-1}$ , respectively. In contrast, the absorption peaks around  $667\text{-}690\text{ cm}^{-1}$  observed by us are related to the vibration of equatorial and axial Te-O bonds in the units of  $\text{TeO}_4$  tbp and  $\text{TeO}_3$  tp [31]. The occurrence of broad peaks is ascribed to the structural mixing of  $\text{TeO}_3$  groups, symmetric  $\text{TeO}_4$  groups and deformed  $\text{TeO}_4$  groups [29, 31-32]. Meanwhile Dousti et al. [20] reported that these bands are broadened with respect to the crystalline  $\text{TeO}_2$  due to the distribution of bond angles and lengths in the amorphous matrix. The bands shift of these groups is highly sensitive to the compositional variation (concentration of  $\text{Er}_2\text{O}_3$ ) within the glass network [30]. The fundamental groups such as OH bond, hydrogen bond and H-O-H bending appear in the higher region [28]. The modification on structure and geometry of ligands with the incorporation of higher  $\text{Er}_2\text{O}_3$  content is evidenced from the peak shift in IR spectra.

#### 4. Conclusion

Our results suggest that the variations in spectroscopic and structural properties of  $\text{TeO}_2$ - $\text{Er}_2\text{O}_3$ - $\text{ZnO}$ - $\text{Na}_2\text{O}$ - $\text{Au}$  glass system can be achieved by varying the concentration of  $\text{Er}_2\text{O}_3$ . The density and refractive index of the glass are found to depend on structural and ligand interactions. The glass forming ability shows excellent enhancement from 0.67 to 0.85 due to the addition of  $\text{Er}_2\text{O}_3$  up to 1.5 mol%. TEM micrograph reveals the presence of Au NPs of average diameter 7.6 nm. The observed UC fluorescence from  $\text{Er}^{3+}$  centers consist of strong and moderate green peaks at 547 and 533 nm accompanied by a relatively weaker red peak at 637 nm wavelength. The two-fold enhancement in the UC luminescence intensity for the sample with 1.0 mol%  $\text{Er}_2\text{O}_3$  is interpreted through different interaction mechanism between coupled metallic NPs-RE ions and excitation beam. The participation of Au NPs as activator in the glass matrix with manipulated  $\text{Er}_2\text{O}_3$  content modifies the glass forming network and also responsible for the changes in the structure and geometry of ligands. We assert that our glass compositions offer a favorable potential to develop the solid state lasers and versatile nanophotonic devices.

#### Acknowledgement

The authors wish to thank to UTM and Ministry of Higher Education (MOHE) for their financial support under Vote 07J80. Asmahani is grateful to MyBrain15 for continuous support.

#### References

- [1] R. de Almeida, D.M. da Silva, L.R.P. Kassab, C.B. de Araujo, Opt. Commun. **281**, 108 (2008).

- [2] Z. Pan, A. Ueda, R. Mu, S.H. Morgan, *J. Lumin.* **126**, 251 (2007).
- [3] R. El-Mallawany, *Mater. Chem. Phys.* **60**, 103 (1999).
- [4] I. Jlassi, H. Elhouichet, S. Hraiech, M. Ferid, *J. Lumin.* **132**, 832 (2012).
- [5] L.R.P. Kassab, M.E. Camilo, C.T. Amancio, D.M. da Silva, J.R. Martinelli, *Opt. Mater.* **33**, 1948 (2011).
- [6] T. Som, B. Karmakar, *Opt. Soc. Am. B.* **26**, B21 (2009).
- [7] H. Hu, Y. Bai, M. Huang, B. Qin, J. Liu, W. Zheng, *Opt. Mater.* **34**, 274 (2011) 274.
- [8] Sh. Zheng, Y. Zhou, D. Yin, X. Xu, X. Wang, *Opt. Mater.* In press (2013)  
DOI: 10.1016/j.optmat.2013.03.017
- [9] H. Zheng, D. Gao, Zh. Fu, E. Wang, Y. Lei, Y. Tuan, M. Cui, *J. Lumin.* **131**, 428 (2011).
- [10] M.Reza Dousti, M.R. Sahar, Raja J. Amjad, S.K. Ghoshal, Asmahani Awang, *J. Lum.*  
DOI: 10.1016/j.jlumin.2013.04.017.
- [11] I. Jlassi, H. Elhouichet, M. Ferid, *J. Mater. Sci.* **46**, 806 (2011).
- [12] T. Som, B. Karmakar, *Plasmonics*, **5**, 149 (2010).
- [13] V.A.G. Rivera, S.P.A. Osorio, D. Manzani, Y. Messaddeq, L.A.O. Nunes, E. Marega Jr., *Opt. Mater.* **33**, 888 (2011).
- [14] U. Kreibig, *Appl. Phys.* **10**, 255 (1976).
- [15] V.A.G. Rivera, D. Manzani, Y. Messaddeq, L. A. O. Nunes, E. Marege Jr., *J. Phys. Conference Series* **274**, 012123 (2011).
- [16] J. Qiu, *Appl. Phys. Lett.* **18**, 3040 (2002).
- [17] H. Kakiuchida, K. Saito, A. J. Ikushima, *Japan. J. Appl. Phys.* **43**, 1743 (2004).
- [18] R.J. Amjad, M.R. Sahar, S.K. Ghoshal, M.R. Dousti, S. Riaz, B.A. Tahir, *Chin. Phys. Lett.* **29**, 087304 (2012).
- [19] Y. Wu, T. Xu, X. Shen, S. Dai, Q. Nie, X. Wang, B. Song, W. Zhang, C. Lin, *IEEE Conference on Industrial Electronics and Applications* 1464 (2011).
- [20] M.R. Dousti, M.R. Sahar, S.K. Ghoshal, Raja J. Amjad, A.R. Samavati, *J. Mol. Struct.* **1035**, 6 (2013).
- [21] A. Abd El-Moneim, *Mater. Chem. Phys.* **73**, 318 (2002).
- [22] M.R. Sahar, A.K. Jehbu, M.M. Karim, *J. Non-Cryst. Solids.* **213 & 214**, 164 (1997).
- [23] K. Kumar, S.B. Rai, D.K. Rai, *Spect. Acta Part A.* **66**, 1052 (2007).
- [24] R.J. Amjad, M. R. Sahar, M. R. Dousti, S. K. Ghoshal, and M. N. A. Jamaludin, *Opt. Express* **21**, 14282 (2013).
- [25] M.R. Dousti, M.R. Sahar, R.J. Amjad, S.K. Ghoshal, A. Khorramnazari, A. Dordizadeh Basirabad, A. Samavati, *Eur. Phys. J. D.* **66**, 237 (2012).
- [26] L.R.P. Kassab, F.A. Bomfim, J.R. Martinelli, N.U. Wetter, J.J. Neto, C.B. de Araujo, *Appl. Phys. B.* **94**, 239 (2009).
- [27] A. Patra, C.S. Friend, R. Kapoor, P.N. Prasad, *J. Phys. Chem. B.* **106**, 1909 (2002).
- [28] K. Selvaraju, K. Marimuthu, *J. Lumin.* **132**, 1171 (2012).
- [29] M.R. Sahar, K. Sulhadi, M.S. Rohani, *J. Mater. Sci.* **42**, 824 (2007).
- [30] P. Gayathri Pavani, K. Sadhana, V. Chandra Mouli, *Phys. B.* **406**, 1242 (2011).
- [31] S. Rosmawati, H.A.A. Sidek, A.T. Zainal, H. Mohd Zobir, *J. Appl. Sci.* **7**, 3051 (2007).
- [32] T. Xu, F. Chen, S. Dai, X. Shen, X. Wang, Q. Nie, C. Liu, K. Xu, J. Heo: *J. Non-Cryst. Solids*, **357**, 2219 (2011).